Appendix

A. Direct numerical simulation of concentric cylindrical shells

A linear theory for small geometric perturbations was formulated for the cylinder by Tomotika [7] and for a cylindrical shell with a cladding of equal viscosity by Stone and Brenner [8]. To develop a quantitative understanding of capillary instability in a cylindrical-shell geometry with a cladding of unequal viscosit, direct numerical simulation is performed using the finite element method using available software (COMSOL). In order to isolate the effect of radial fluctuations, we impose cylindrical symmetry, so the numerical simulation simplifies into a 2D problem in the (r,z) plane. Numerical challenges in the simulations arise from the nonlinearity, moving interfaces, interface singularities, and the complex curvature [1,45]. A level-set function $\phi(\vec{x},t)$ is coupled with the NS equations to track the interface [46–49], where the interface is located at the $\phi = 0.5$ contour and the ϕ evolution is given by $\vec{u}$ via:

$$\phi_t + \vec{u}\cdot\vec{\nabla}\phi = 0. \tag{13}$$

The local curvature (κ) at an interface is given in terms of ϕ by:

$$\kappa = \nabla\cdot\vec{n} = \nabla\cdot\frac{\nabla\phi}{|\nabla\phi|} = \frac{(\phi_r^2\phi_{zz}+\phi_z^2\phi_{rr})+(\phi_r^2+\phi_z^2)\phi_r/r-\phi_r\phi_z(\phi_{rz}+\phi_{zr})}{(\phi_r^2+\phi_z^2)^{3/2}}. \tag{14}$$

In the simulation, the level set function is defined by a smoothed step function reinitialized at each time step [49]. A triangular finite-element mesh is generated, and second-order quadratic basis functions are used in the simulation.

The evolution of a capillary instability can be obtained from direct numerical simulation. Figures 7(i)–7(v) presents snapshots of the flow field and interface. (i) Initially, the pressure of the inner fluid is higher than that of the outer fluid due to Laplace pressure ($p = \gamma\kappa$) originating from azimuthal curvature of the cylindrical geometry at interfaces I and II. (ii)–(iv) The interfacial perturbations generate an axial pressure gradient Δp, and hence a fluid flow occurs that moves from a smaller-radius to a larger-radius region for the inner fluid. Gradually the amplitude of the perturbation is amplified. (v) The*shrunk* smaller-radius and *expanded* larger-radius regions of inner fluid further enhance the axial pressure gradient Δp, resulting in a larger amplitude of the perturbation. As a result, the small perturbation is exponentially amplified by the axial pressure gradient.

We investigate the dependence of instability timescale on cladding viscosity (η_{clad}) with a fixed shell viscosity (η_{shell}), in order to help us to identify suitable cladding materials for fiber fabrication. The time-dependent perturbation amplitude curves for various viscosity contrast $\eta_{\text{clad}}/\eta_{\text{shell}}$ are obtained by changing the cladding viscosity ($\eta_{\text{shell}} = 10^5$ Pa$\cdot$s). (Other parameters in the simulation are $\rho = 10^3$ kg/m^3, $\gamma = 0.6$ N/m, $R = 120$ μm.) Instability time scale for the each given viscosity contrast is obtained by exponentially fitting the curves of time-dependent instability amplitude. Instability time scale (τ) as a function of viscosity contrast is presented in Fig. 3. The existing linear theory has only been solved in case of equal viscosity, and predicts that the instability time scale is proportional to the viscosity $\tau \sim \eta$ [8]. We obtain a more general picture of the instability time scale for unequal viscosity by considering two limits. In the limit of negligible cladding viscosity, $\eta_{\text{clad}} \to 0$, the instability time scale should be determined by η_{shell}, and from dimensional analysis should be proportional to $r\eta_{\text{shell}}/\gamma$, assuming that the inner and outer radius are comparable and so we take r to be the average radius. In the opposite limit of $\eta_{\text{clad}} \to \infty$, the time scale should be determined by η_{clad} and hence should be proportional to $r\eta_{\text{clad}}/\gamma$. In between these two limits, we expect the time scale to smoothly interpolate between the $r\eta_{\text{shell}}/\gamma$ and $r\eta_{\text{clad}}/\gamma$ scales. In a companion paper [34],

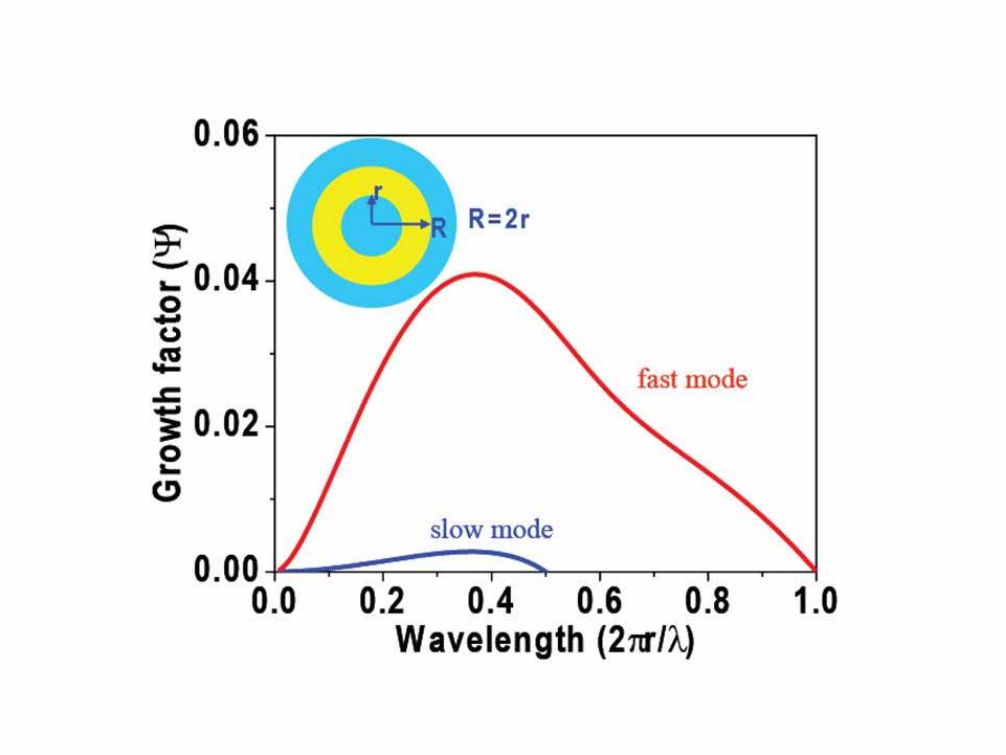

Fig. 8. Growth factor of instability as a function of perturbation wavelength. Fast- and slow- modes occur at wavelengths above their respective critical wavelengths λ_f, λ_s. Inset is a sketch of coaxial cylinder with radius $R = 2r$ and equal viscosities.

we present a generalized analytical linear theory for multi-fluid cylindrical structures, and show that this dimensional analysis is consistent with the exact asymptotic result.

B. Linear theory of concentric cylindrical shells with equal viscosities

A linear theory of capillary instability for a co-axial cylinder with equal viscosities is provided in the literature by Stone and Brenner [8]. The growth rate (σ) for a wave vector $k = 2\pi/\lambda$ is a solution of the following quadratic equations

$$\left\{\sigma - \frac{k^2\gamma_1}{r\eta}\left[1-(rk)^2\right]\Lambda(r,r)\right\} \times \left\{\sigma - \frac{k^2\gamma_2}{R\eta}\left[1-(Rk)^2\right]\Lambda(R,R)\right\} = \frac{k^4\gamma_1\gamma_2}{rR\eta^2}\left[1-(rk)^2\right]\left[1-(Rk)^2\right]\Lambda(r,R)^2, \quad (15)$$

where r and R are the radii of the unperturbed interfaces I and II, γ_1 and γ_2 are the interfacial tensions, and η is viscosity. $\Lambda(a,b)$, where $a \leq b$, is associated with the modified Bessel function,

$$\Lambda(a,b) = \int_0^\infty \frac{sJ_1(sa)J_1(sb)}{(s^2+k^2)^2}ds - \frac{1}{2k}\frac{d}{dk}\left[I_1(ak)K_1(bk)\right]. \quad (16)$$

For the case of $\gamma_1 = \gamma_2 = \gamma$, the growth rate has the following formula,

#148521 - $15.00 USD Received 31 May 2011; revised 25 Jul 2011; accepted 1 Aug 2011; published 10 Aug 2011

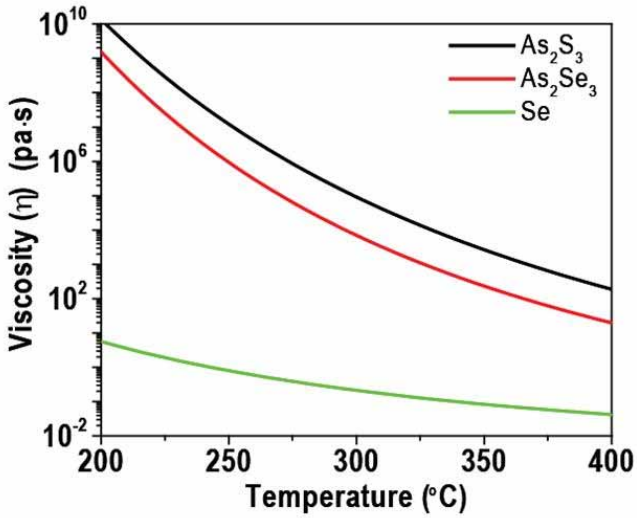

Fig. 9. Temperature-dependent viscosity for various chalcogenide glasses. Typical temperature during fiber drawing for glass Se, As_2Se_3, As_2S_3 is around $220, 260, 300$ ^oC with the corresponding viscosities of $10, 10^5, 10^5$ $Pa \cdot s$, respectively.

$$\sigma(\lambda) = \frac{\gamma}{\eta r}\Psi(\lambda, R/r), \tag{17}$$

where the growth factor of $\Psi(\lambda, R/r)$ in Eq. (17) is a complicated function of instability wavelength [8]. The instability time scale $\tau \sim \sigma^{-1} \sim \eta r/\gamma$ is scaled with radius. For the case of $R = 2r$, this growth factor is calculated in Fig. 8. A positive growth factor indicates a positive growth rate ($\sigma > 0$), for which any perturbation is exponentially amplified with time. Instability occurs at long wavelengths above a certain critical wavelength. Two critical wavelengths exist for the co-axial cylinder shell. One is a short critical wavelength $\lambda_f = 2\pi r$ for a faster-growth mode (red line). The other is a long critical wavelength $\lambda_s = 2\pi R$ for slower-growth mode (blue line).

C. Viscosity of Materials During Thermal Drawing

Our chosen materials include chalcogenide glasses (Se, As_2Se_3, and As_2S_3) and thermoplastic polymers (PES, PEI, and PSU). The viscosity of chalcogenide glass-forming melts depends on temperature and is calculated from an empirical Arrhenius formula [50],

$$\log\eta = \log\eta_0 + C\frac{exp(D/T)}{2.3RT} - 1, \tag{18}$$

where R is the ideal gas constant, T is the temperature in Kelvin, and η is viscosity in $Pa \cdot s$. The parameters of $\log\eta_0$, C, and D for our materials are listed below: $-2.0, 6651, 770.82$ for Se,

#148521 - $15.00 USD Received 31 May 2011; revised 25 Jul 2011; accepted 1 Aug 2011; published 10 Aug 2011

$-3.09, 18877.8, 875.56$ for As_2Se_3, and $-3.62, 33744, 650.8$ for As_2S_3 [51]. These viscosities over a wide temperature range are plotted in Fig. 9. The typical temperature during a fiber drawing for Se, As_2Se_3, or As_2S_3 films is around $220, 260$, or $300\ ^oC$, respectively, with the corresponding viscosities of $10, 10^5$, or $10^5\ Pa \cdot s$, respectively.

Acknowledgments

This work was supported by the Center for Materials Science and Engineering at MIT through the MRSEC Program of the National Science Foundation under award DMR-0819762, and by the U.S. Army through the Institute for Soldier Nanotechnologies under contract W911NF-07-D-0004 with the U.S. Army Research Office.

#148521 - $15.00 USD Received 31 May 2011; revised 25 Jul 2011; accepted 1 Aug 2011; published 10 Aug 2011